(7) C. Dismukes and Y. Siderer published the first observation of an EPR signal attributable to a multinuclear Mn center in PS II (Proc. Natl. Acad. Sci. USA (1981) 78, 274-278)

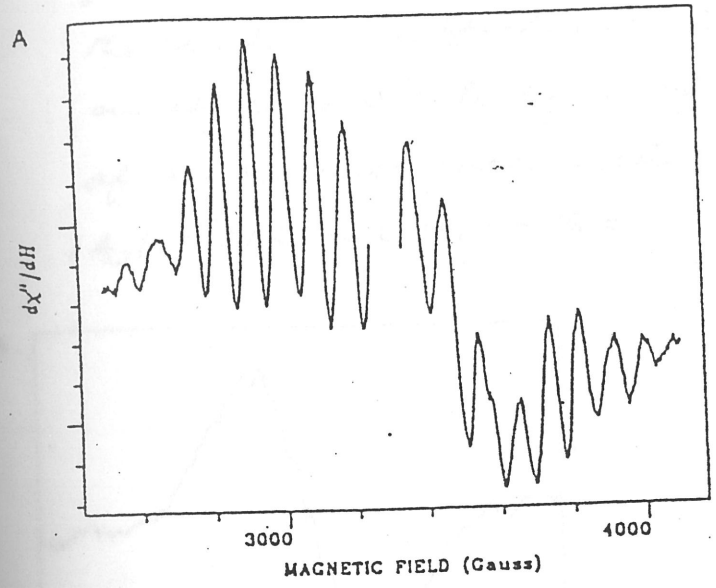

observed in dark-adapted spinach chloroplasts that were subjected to a series of light flashes & quickly frozen. A single flash gave an EPR at $g \sim 2$, with at least 16 partially resolved hyperfine lines with a regular interpeak separation of ~ 80 G. EPR amplitude was diminished by a second, third or fourth flash, increased following a fifth flash and diminished again a sixth flash, thus following the period dependence of the Kok S-state cycle

$g \simeq 2$ "multiline" EPR signal (19 or more partially Mn hyperfine lines)

The above $g \simeq 2$ "multiline" signal is assigned to "S_2" state.

(8) J. L. Casey and K. Sauer (Biochim. Biophys. Acta (1984) 767, 21-28) and J. L. Zimmerman and A. W. Rutherford (BBA (1984) 767, 160-167) have reported the formation of another light-induced EPR signal in PS II-enriched membranes.

This signal is centered at $g \sim 4.1$ (linewidth 320 G)

Casey and Sauer obtained this signal by continuous illumination at 140 K. Zimmerman & Rutherford observed $g \sim 4.1$ signal in PS II membranes illuminated at 200 K in presence of sucrose. They showed that the amplitude of this signal followed the same flash number dependence as

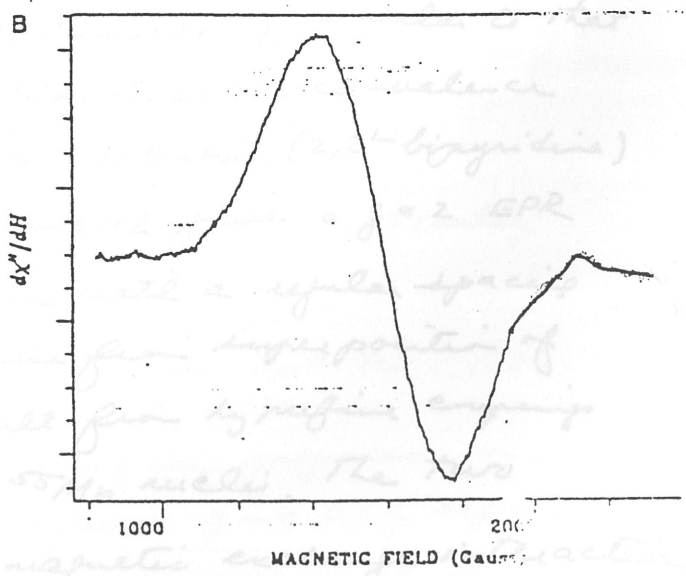

(9) Recently M. Klein, K. Sauer and coworkers (JACS 112 9389-9391 (1990)) showed that the g = 4.1 EPR signal also exhibits Mn hyperfine when the signal is recorded on oriented PS II membranes. At least 16 Mn hyperfine features are resolved, indicating <u>at least</u> two Mn for the cluster. The spectrum could be simulated utilizing an effective $S' = 1/2$ system of an $S = 3/2$ or $S = 5/2$ spin state of an Mn tetranuclear structure with $|A_1| = 47$ G, $|A_2| = 37$ G, $|A_3| = 34$ G and $|A_4| = 16$ G.

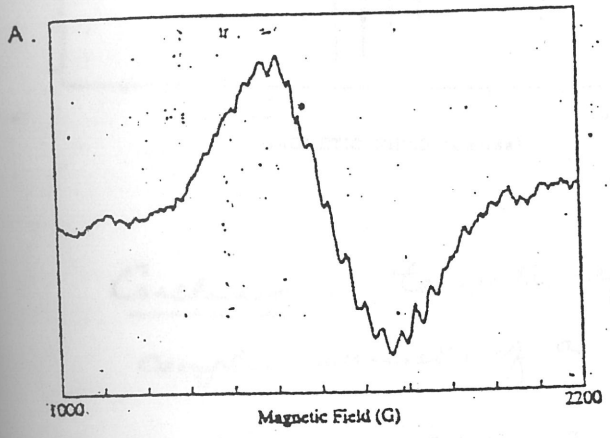

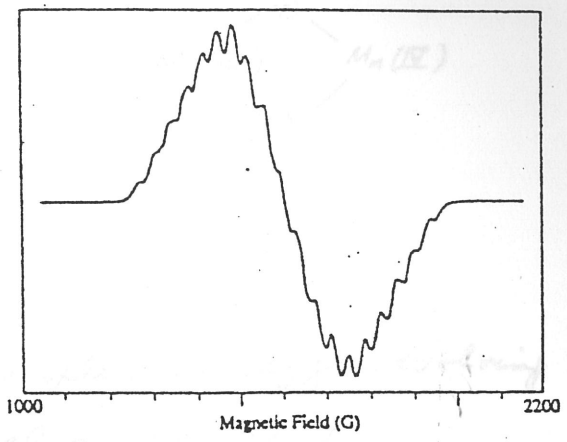

(A) EPR spectrum of oriented PSII membranes with 100 m*M* NH_4Cl at pH 7. the presence of 400 m*M* sucrose. The membrane normal is oriented parallel to the app magnetic field (0°). The dark S_1 state spectrum has been subtracted from the S_2 state EPR si recorded following 5 min illumination at 195 K. The peak labeled with an asterisk subtraction artifact. Spectrometer conditions are as follows: microwave frequency, 9.22 G microwave power, 20 mW; field modulation amplitude, 10 G; sample temperature, 8 (B) Simulation of the spectrum in (a) utilizing an effective $S' = 1/2$ system and Gaus lineshapes. The following isotropic parameters were used: $g = 4.1$; $\Delta_{hwhm} = 16$ G; $|A_1| =$ G, $|A_2| = 37$ G, $|A_3| = 34$ G, $|A_4| = 16$ G. The reduced hyperfine couplings are consistent an $S = 3/2$ or $S = 5/2$ spin state of an Mn tetranuclear structure. (Figure adapted from ref. 3

(10) The g = 2 "multiline" EPR signal must arise from a Mn cluste as well (16 or more hyperfine lines; <u>six only</u> for one Mn!), containing <u>at least</u> two Mn (i.e., binuclear), similar to that observed in the EPR spectra of binuclear mixed-valence Mn compounds, e.g. the di-μ-oxo-tetrakis(2,2'-bipyridine) dimanganese(III,IV) perchlorate, which gives a g = 2 EPR signal with 16 well-resolved lines with a regular spacing of ~80 G. Here the 16 lines arise from superposition of 36 nearly isotropic lines that result from hyperfine coupling to the two nonequivalent $I = 5/2$ ^{55}Mn nuclei. The two oxygen bridges a strong antiferromagnetic exchange interaction

between the $S = 3/2$ Mn(III) and the high-spin [Mn (III) ($S = 2$)

so that the effective spin is $S_T = 1/2$

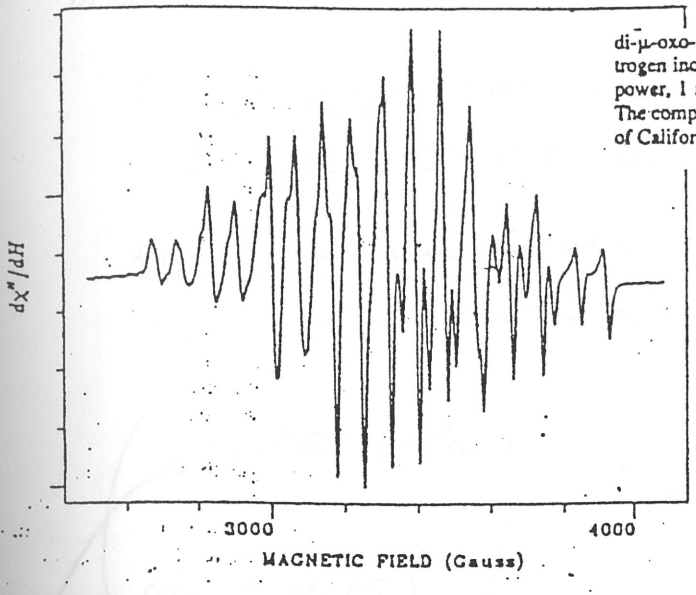

The continuous-wave EPR spectrum for the mixed valence bina[illegible] Mn co[illegible] di-μ-oxo-tetrakis(2,2'-bipyridine)dimanganese(III,IV) perchlorate with the [illegible] nitrogen incorporated into the 2,2'-bipyridine ligands. Frequency, 9.2 GHz; temperature, [illegible] K; power, 1 mW; modulation amplitude, 1.0 G. (Figure kindly provided by Dr. V[illegible] DeRose.) The compound was synthesized by Dr. Michael Chan and Prof. W. H. Armstrong (University of California, Berkeley).

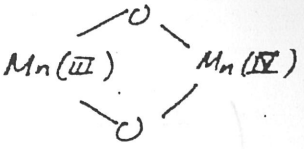

Conclusion: the water-splitting complex or oxygen evolving complex consists of a multinuclear Mn cluster

→ More on the multinuclearity of the Mn cluster

There has been considerable controversy over this issue!

What is definite is that it is not mononuclear!

The following proposals have been put forth.

(1) Binuclear

Mixed valence Mn(II) Mn(III) antiferromagnetically coupled cluster

$S_1 = \frac{5}{2}$ $S_2 = 2$ ⟶ $S_T = 1/2$

or Mixed valence Mn(III) Mn(IV) antiferromagnetically coupled cluster

$S_1 = 2$ $S_2 = 3/2$ ⟶ $S_T = 1/2$

Many of such model complexes have been prepared over the past decade, all of which exhibit a $g \sim 2$ EPR signal with hyperfine interaction approaching that of the $g = 2$ EPR

multiline line, but not a perfect match. The g=2 "multiline" EPR signal from PS II membranes exhibits 19 or more partially resolved hyperfine lines rather than 16 typically observed for mixed valence binuclear Mn complexes.

(2) Trinuclear (Ö. Hansson, R. Aasa, and T. Vänngård, Biophys. J. (1987) 51, 825–832)

Redox equilibrium between an isolated Mn(III) ($S_1 = 3/2$) and a binuclear Mn site ($S_{23} = 1/2$), e.g.

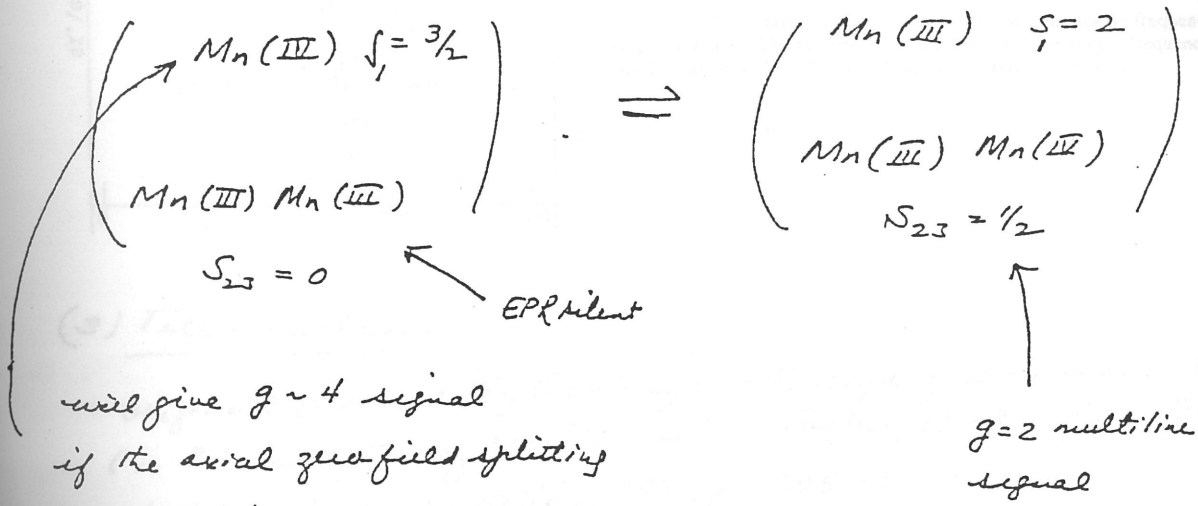

will give g ~ 4 signal if the axial zero-field splitting $D >> g\beta H$ has been observed in mononuclear Mn(IV) models

This proposal is now ruled out by the Mn hyperfine pattern observed for the g = 4.1 signal (too many lines). Also, A. Haddy, W.R. Dunham, R.H. Sands and R. Aasa have now recorded the spectra at three frequencies and the shift in g-value at the higher frequency is inconsistent with the S=3/2 model. Instead the results indicate that the signal arises from the middle doublet of an $S = 5/2$ multiplet.

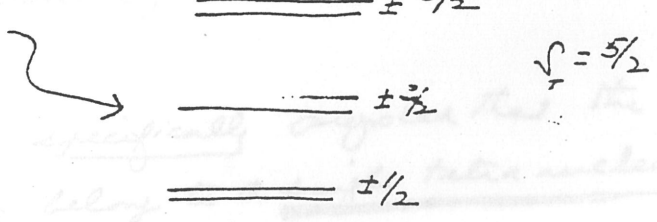

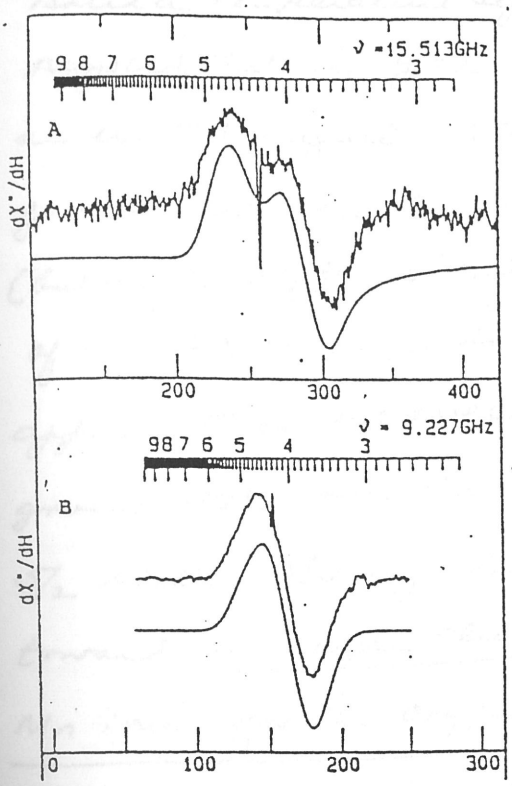

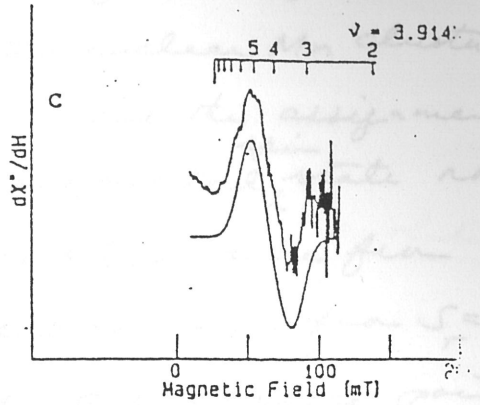

Comparison of the $g = 4$ signal at three microwave frequen[illegible] and (C) 3.9 GHz. The simulated spectra (bottom curve at each frequency [illegible] Hamiltonian with $S = 5/2$, $D = 0.43\ cm^{-1}$, and $E/D = 0.25$.

(3) Tetranuclear

originally proposed by Govindjee, T. Wydrzynski and S. B. Marks (in "Bioenergetics of Membranes", L Packer, et al, Eds. Elsevier/North Holland, Amsterdam, 1977, pp 305-316)

J.C. de Paula, J. B. Innes and Gary Brudvig (Biochemistry 1985, 24 8114-8120) and J. L. Zimmerman and A. W. Rutherford (Biochemistry 1986, 25, 4609-4615) proposed that the g=2 multiline and the g = 4.1 signals arise from a common Mn site, with an interconversion between signals based on temperature-dependent structural changes, i.e., the signals arise from different magnetic spin states of a single multinuclear Mn cluster, with the conversion between spin states triggered by slight conformational changes of the cluster induced by the use of different cryoprotectants.

J.C. de Paula and Gary Brudvig specifically proposed that the two different magnetic spin states belong to a single tetranuclear Mn cluster! (J Am Chem Soc. (1985) 107, 2643-2648)

Based on temperature dependence, de Paula and G. Brudvig proposed that the g=2 multiline signal originated from an excited magnetic state, and the g=4.1 signal to the ground state of the ~~———~~ tetranuclear Mn cluster (but slightly different configuration). But this assignment of the g=2 multiline signal to an excited spin state now appears to be incorrect. Most likely, it arises from $S_T = 1/2$ ground state, and the g=4.1 signal arises from $S_T = 3/2$ or $5/2$ states. In any case, all the EPR evidence points toward a single cluster of four magnetically coupled Mn ions for the oxygen-evolving complex!

→ Proposals for mechanism of dioxygen evolution

next lecture

→ More on the Mn cluster in photosynthesis

→ Nitrogenase

→ Long-range electron transfer

- Photosynthesis and Photo oxidation of Water (Continue)

→ Mechanisms proposed for H_2O oxidation and O_2 evolution

(1) Although there appears to be now consensus that the water-splitting complex or oxygen evolving complex is a tetranuclear Mn cluster, we know very little of its structure, including the detailed arrangement of the manganese ions in the cluster, the ligand structure, not to mention the three-dimensional structure. This paucity of structural data has not held back people from proposing mechanisms for the H_2O oxidation. A number of proposals based on the tetranuclear Mn cluster have now been put forth, and I would like to conclude this discussion with some of these ideas in the hope that they will stimulate you to come up with even better ones, and better yet, inspire those of you who are synthetic chemists to go into the lab to synthesize model Mn clusters that will more closely mimic the cluster or catalyst in the green plant or cyanobacteria.

(2) Constraints on the structure imposed by EPR, XAS and EXAFS

(a) EPR

S_2: Based on $g \doteq 2$ multiline EPR observed for the cluster in the "S_2" state, the cluster in this state must contain an odd number of electrons. EPR studies of model Mn dinuclear mixed valence complexes as well as simulation of the EPR multiline signal indicate that the Mn in the cluster is in a mixed-valence complex

involving oxidation states (II, III) or (III, IV)

S_1 : integer spin system (even number of electrons)

A parallel polarization EPR signal has been observed by S.L. Dexheimer, K. Sauer and M.P. Klein (JACS 1993) at $g = 4.8$

A similar EPR (integer spin parallel polarization) signal has been observed for $[(Mn_2O_2)_2(tphpn)_2]^{4+}$ (III, IV) - (III, IV) "dimer of dimers" prepared by M. Cheng & W. Armstrong (JACS (1991) 113, 5053-5057).

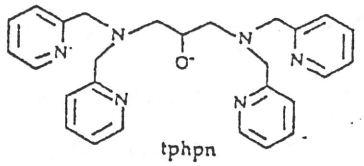

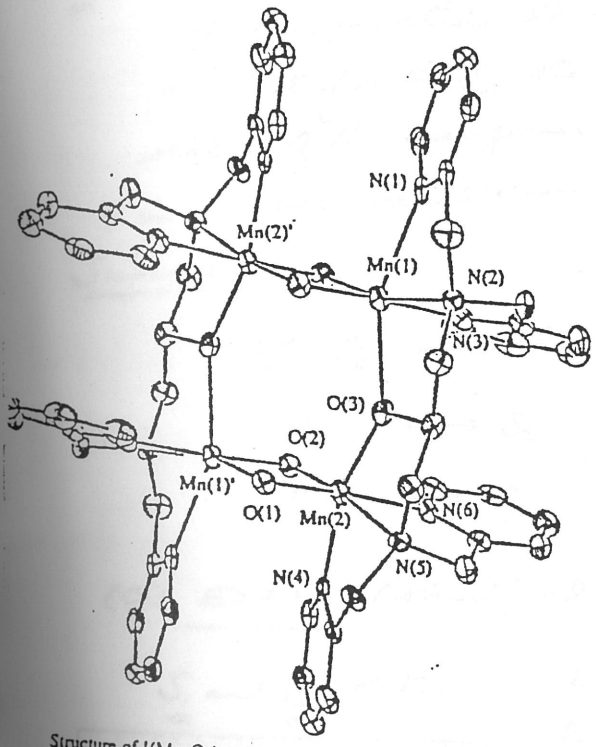

Structure of $[(Mn_2O_2)_2(tphpn)_2]^{4+}$

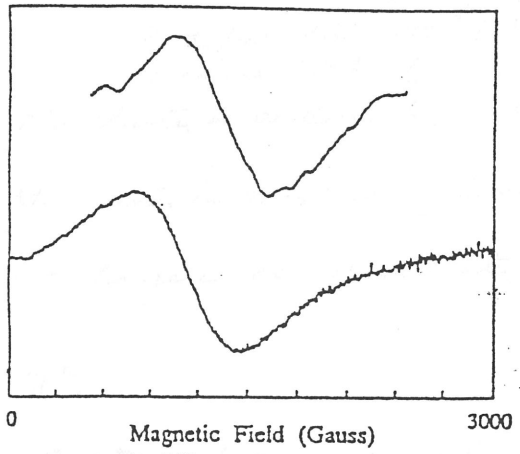

Photosystem II Oxygen-Evolving Complex at S_1

$[(Mn_2O_2)_2(tphpn)_2]^{4+}$ (III,IV)-(III,IV) "dimer of dimers"

Top: Difference EPR spectrum of the spinach photosystem II S_1 state.[5] Bottom: X-band (ν = 9.25 GHz) EPR spectrum of $[(Mn_2O_2)_2(tphpn)_2]^{4+}$ (17) in CH_3CN at 4 K employing parallel polarization geometry. Reprinted with permission from ref 49. Copyright 1991 American Chemical Society.

(b) X-ray Kedge spectroscopy

S_2 : From a comparison of the Mn Kedge inflection energy of a series of Mn complexes with PS II preparations, it has been concluded that the Mn atoms in the OEC (oxygen evolving complex) in the S_2 state are predominantly in the (III) and IV oxidation states.

S_1 : The Kedge energy shifts to higher energy by ~1 eV when

the OEC is advanced from the S_1 to the S_2 state, indicating that the oxidation state of the Mn complex increases. From comparison with model compounds, it has been suggested that the change from S_1 to S_2 corresponds to a one-electron oxidation.

S_0^*: This is an S_0-like state, which can be induced by incubation with NH_2OH followed by illumination. The K edge of the S_0^* is shifted to lower energy by ~1 eV relative to the S_1 state, suggesting storage of an oxidative equivalent within the Cluster during the S_0^* to S_1 transition.

S_3: When the PS II preparations are poised in the S_3 state following low temperature illumination, the Mn K edge is the same as that for the S_2 state, implying no change in the oxidation states of the manganese ions and storage of the oxidizing equivalent in an associated amino acid "ligand." A histidine appears to be oxidized (EPR at $g = 2.004$)

A. Rutherford Nature (1990) 347, 303-306
C. Dismukes Biochemistry (1990) 29, 10814-10822

Summary

$S_0^*, S_0 \longrightarrow S_1$ Mn cluster is oxidized by 1 oxidizing equivalent

$S_1 \longrightarrow S_2$ Mn cluster is oxidized by 1 oxidizing equivalent

$S_2 \longrightarrow S_3$ no change in oxidation state of Mn ions

(C) EXAFS (structural change

S_1 and S_2 states:

2 N or O atoms / Mn at 1.8 Å
2 to 4 O or N atoms / Mn at 1.9 - 2.2 Å
1 to 1.5 Mn / Mn at 2.7 Å
0.5 Ca or 0.5 Mn / Mn at 3.3 Å

Essentially no structural change between S_1 & S_2

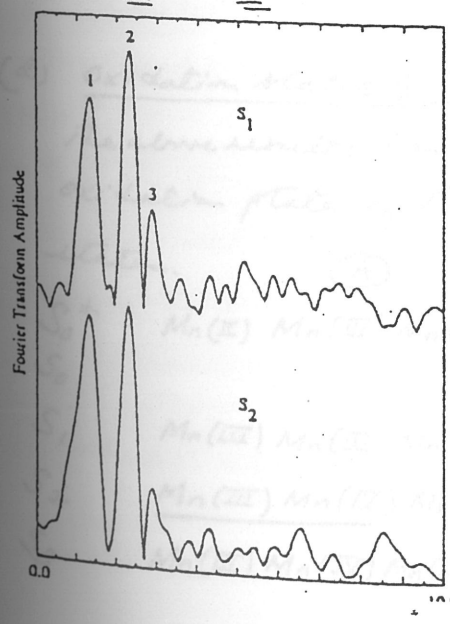

The Fourier transform of the k^3-weighted EXAFS data from *Synechococcus*. Peak 1 is backscattering from bridging and terminal ligand N or O atoms at about 1.8 and 1.9–2.2 Å. Peak 2 is Mn at 2.7 Å and peak 3 fits to C, Ca, or Mn at about 3.3 Å. The data were collected at 10 K using a 13 element Ge detector. The data from spinach PSII preparations are similar to those shown here. Note the subtle differences in the intensities of the peaks labeled 1 and 2 in the S_1 and S_2 states.

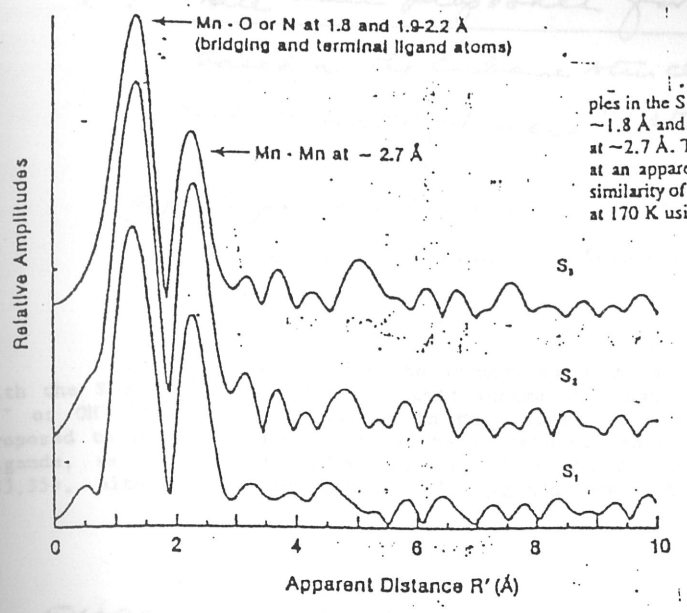

. Fourier transforms of the k^1-weighted Mn EXAFS data of spinach PSII samples in the S_1,S_2, and S_3 states. The first peak is primarily due to bridging O (or N) ligands at ~1.8 Å and terminal O (or N) ligands at 1.9–2.2 Å. The second peak is primarily due to Mn at ~2.7 Å. These peaks are characteristic of a di-μ-oxo-bridged Mn cluster. The peaks appear at an apparent distance R', which is shorter than the real internuclear distance. Note the similarity of the Fourier transforms in the S_1, S_2, and S_3 states. The EXAFS data were collected at 170 K using a single element Si–Li detector.

No significant structural changes between S_1, S_2 and S_3 states!

But significant structural differences between S_0^* and S_1

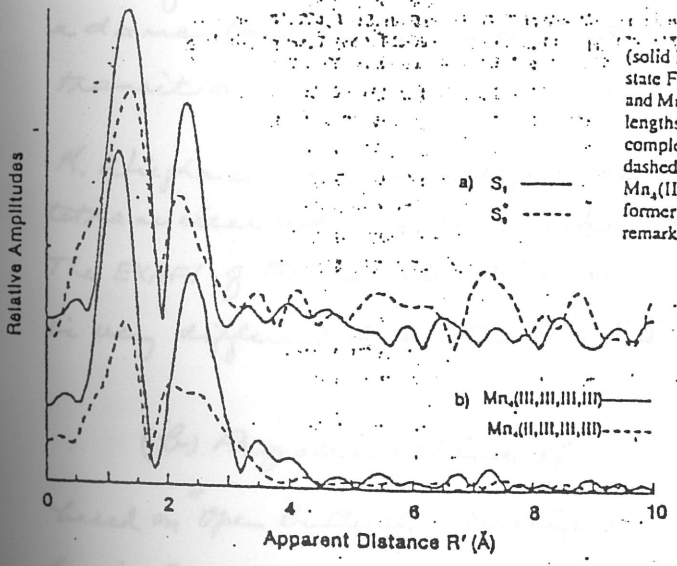

. (a) Fourier transforms of the k^1-weighted Mn EXAFS of an S_1 state preparation (solid line) and S_0 state preparation (dashed line). The significantly lower amplitude of the S_0 state Fourier transform indicates a more disordered system, with a larger spread in Mn–O, N, and Mn–Mn distances. The distances R' in the Fourier transforms are shorter than the true bond lengths. (b) The Fourier transforms of the k^1-weighted Mn EXAFS of a tetranuclear Mn complex $Mn_4(III,III,III,III)$ $(\mu_3\text{-}O)_2$ $(\mu_2\text{-}Bz)_7$ $(bipy)_2$ (ClO_4) is shown as the solid trace. The dashed line is the Fourier transform of an isostructural manganese tetranuclear complex $Mn_4(II,III,III,III)$ $(\mu_3\text{-}O)_2$ $(\mu_2\text{-}Bz)_7$ $(bipy)_2$, which contains one Mn(II) ion not present in the former isostructural complex. Note that the reduction in the amplitude of the Fourier peaks is remarkably similar to that observed between the S_1 and S_0 states.

(d) Oxidation states of the Mn ions in various S states

The above results have led to the following proposals for the oxidation states of the Mn ions in the OEC in the various "S" states.

	(A)	(B) favored
S_0^*	Mn(II) Mn(III) Mn(III) Mn(III)	Mn(II) Mn(III) Mn(IV) Mn(IV)
S_0		
S_1	Mn(III) Mn(III) Mn(III) Mn(III)	OR Mn(III) Mn(III) Mn(IV) Mn(IV)
S_2	Mn(III) Mn(IV) Mn(III) Mn(III)	Mn(III) Mn(IV) Mn(IV) Mn(IV)
S_3	Mn(III) Mn(IV) Mn(III) Mn(III)	Mn(III) Mn(IV) Mn(IV) Mn(IV)

(3) Three main proposals for the mechanism of water oxidation based on the cubane structure (a), butterfly structure (b) and "dimer-of-dimers" structure (c) for the Mn cluster

(a) Proposed Scheme of G.W. Brudvig and R.H. Crabtree (Proc. Natl. Acad. Science. USA (1986) 83, 4586–4588)

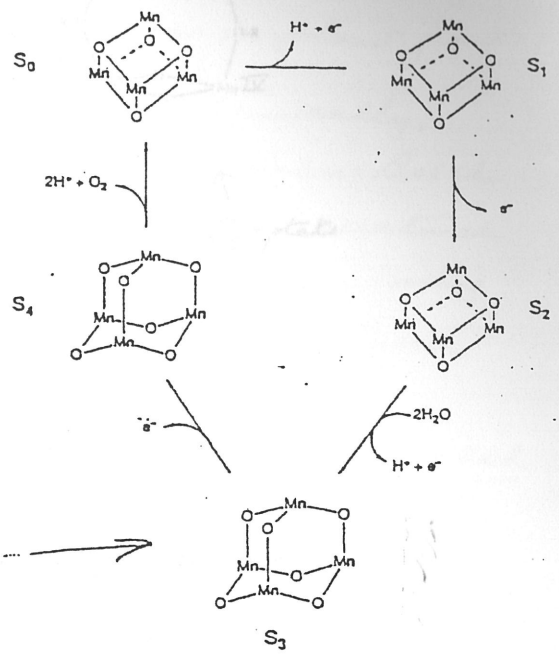

A proposed scheme for the structures of Mn associated with the S state transitions. In this scheme, O denotes either O^{2-} or OH^- ligands. Each Mn ion in the tetrameric complex is proposed to also be coordinated to the protein via three O or N ligands, as indicated by EXAFS studies of Mn in the S_1 state (33,35), although the protein-derived ligands are not shown.

EXAFS (lack of significant change accompanying the S_2 to S_3 transition) argue against structural rearrangement from a cubane-like to adamantane-like structure during S_2–... transition

K. Wieghardt has synthesized a tetranuclear adamantane-like Mn complex. The EXAFS of this complex shows a Mn...Mn distance of 3.2 Å, which is very different from that PS II in S_3 state!

(b) Proposed scheme of G. Christou and J.B. Vincent (BBA (1987) 895 259–274)

based on "open butterfly" structures for the S_0 and S_1 states and structural arrangements in the $S_1 - S_2$ and $S_2 - S_3$ transitions where the "open butterfly" is transformed into a distorted cubane-like structure

EXAFS argues against this scheme also!

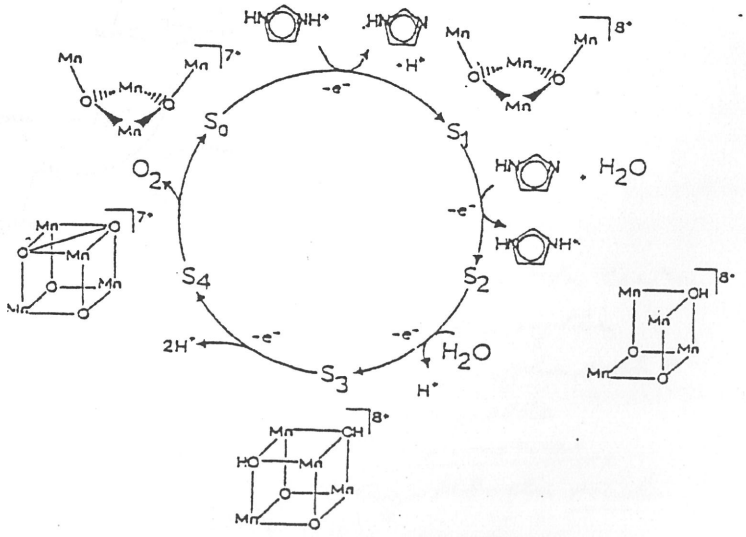

Proposed mechanistic scheme for water oxidation employing the Mn_4O_2 and Mn_4O_3 cores established in model complexes.

(c) Scheme proposed by M. Cha and W. Armstrong based on the "dimer of dimers" structure

(i) O···O bond formation within a di-μ-oxo unit

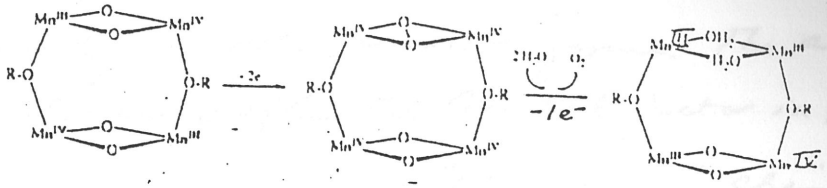

S_1-state S_2-state S_0-state

(two weakly interacting $Mn(III)$–O–O–$Mn(IV)$)

$S_{Mn} = 1/2$ $S_{Mn} = 1/2$

$S_T = 0$ or 1

(ii) O··· O bond formation between two di-μ-oxo units

S_2

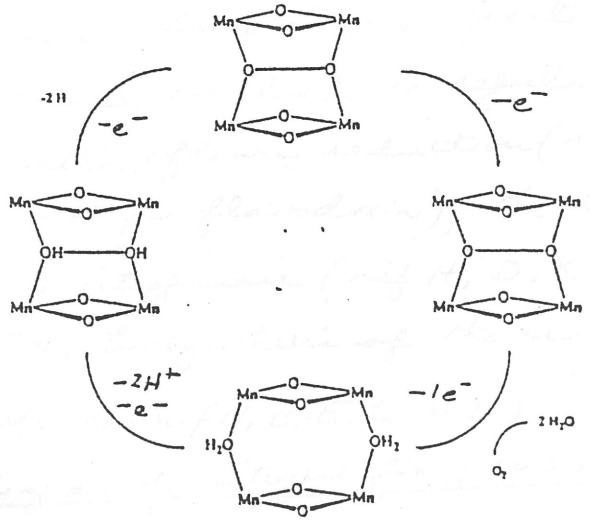

S_1 S_3

S_0

• Nitrogenase and Nitrogen Fixation

→ The process of nitrogen fixation is an essential part of the nitrogen cycle on the planet earth. It is estimated that >60% of the N_2 that is ultimately converted to NH_4^+ is done so by the nitrogenase enzyme. The availability of fixed nitrogen is often the limited factor in plant growth.

→ Man has developed processes to "fix nitrogen" chemically. The most important process in use today is the Haber-Bosch process in which N_2 and H_2 are reacted at temperatures between 300–500°C and pressures over 300 atm using Fe-based catalysts. 1000 tons of NH_3 / day are produced at several hundred plants in this fashion.

→ In the biological process, N_2 is reduced locally <u>as needed</u> at room temperature and ~0.8 atm pressure. This reduction is accomplished by the enzyme, nitrogenase, a highly complicated enzyme complex, coded by <u>at least</u> seventeen genes. These nitrogen fixation (nif) genes specify proteins that are involved in regulation (nifA and L), pyruvate oxidation / flavin reduction (nifJ), electron transfer (nifF for flavodoxin), the subunits of the structural proteins of the nitrogenase (nifH, D, K), Fe-S cluster assembly (nifM) and the biosynthesis of the iron molybdenum cofactor, FeMo-co (nifN, B, E, Q, V, H) see next page

→ <u>Schematic diagram of nitrogen-fixing enzyme</u>

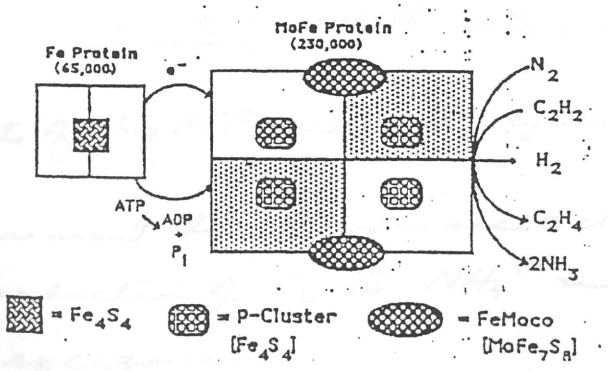

present in certain prokaryotes (diazotrophs such as *Klebsiella pneumoniae*, *Azotobacter vinelandii* or *Clostridium pasteurianum*

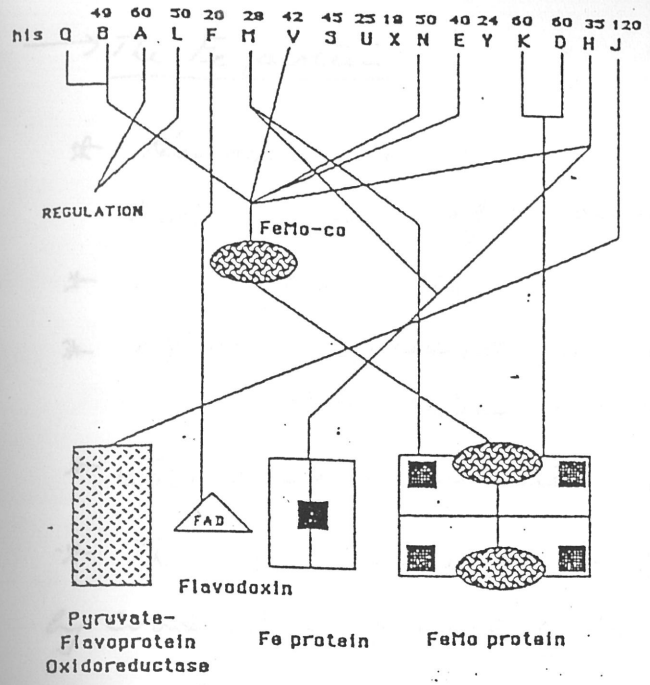

Nif genes required for nitrogen fixation as arranged in Klebsiella pneumoniae. The numbers in the top row are molecular weights in kilodaltons of the protein gen products of the respective *nif* genes whose letters are show below them.

→ Overall reaction

Nitrogenases from Klebsiella pneumoniae, Azotobacter Vinelandii, Clostridium pasteurianum catalyze the reduction of dinitrogen to ammonia in a reaction that is coupled to the evolution of H_2 and the hydrolysis of ATP.

Under optimum conditions in vitro, the stoichiometry for the reaction is given by

$$N_2 + 8H^+ + 8e^- + 16\,MgATP \xrightarrow{\text{nitrogenase}} 2NH_3 + H_2 + 16\,MgADP + 16\,P_i$$

Reductant: in vivo flavodoxin or ferrodoxin

in vitro dithionite, or viologens

Two equivalents of MgATP are hydrolysed per electron!

The ATP requirement for nitrogenase activity is intriguing because the reduction of N_2 to NH_4^+ under physiological conditions is exergonic.

$$N_2 + 0.25\,glucose + 2H^+ + 1.5H_2O \longrightarrow 2NH_4^+ + 1.5CO_2$$

$$\Delta G^{\circ\prime} = -117\ kJ/mol\ of\ N_2\ reduced$$

→ The Fe protein

* Homodimer (α_2)
  - Molecular mass of subunit ~ 30 kDa (28 – 36 kDa)
* Product of the nifH gene
* nifM gene product (27–28 KDa) also involved in processing of iron protein — assembling Fe–S cluster
* Five conserved cysteins
* The two subunits are held together by a Fe_4S_4 cubane cluster by coordination of each of the four Fe atoms to either a Cys-97 or a Cys-132 located in each subunit.

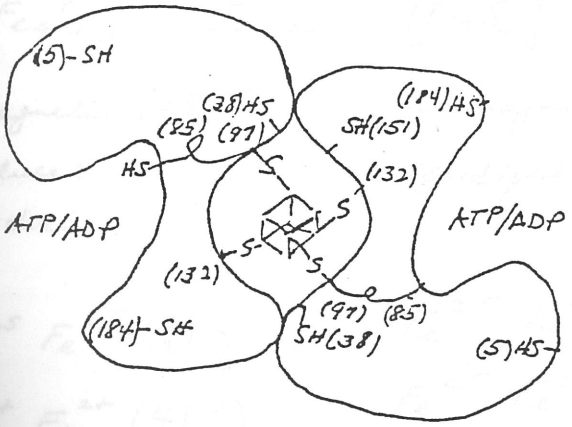

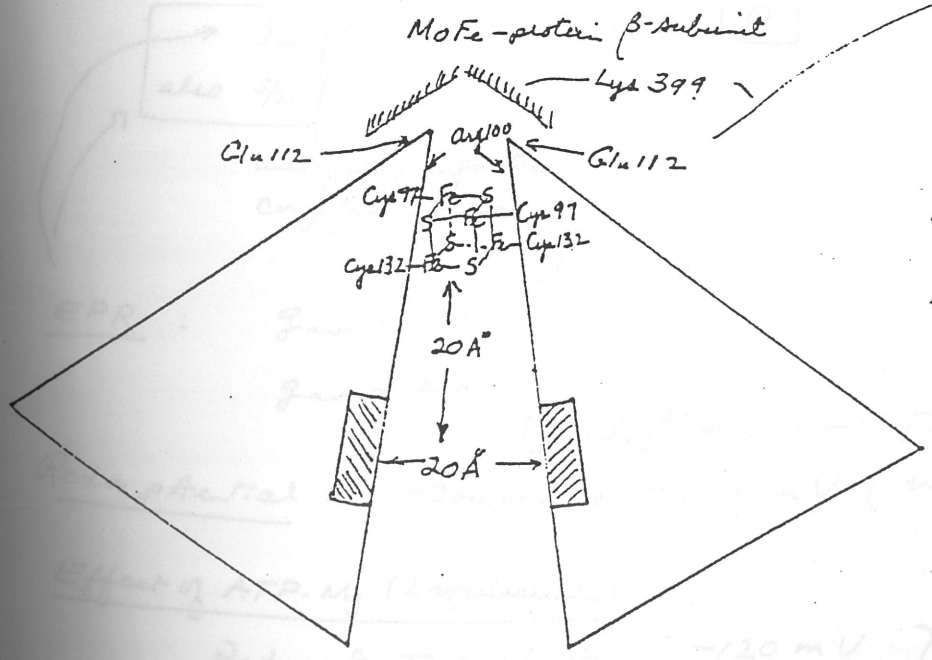

Glu 112 interacts with Lys 399

Arg 100 (close to Fe_4S_4 on surface) becomes ADP-ribosylated as part of a regulatory mechanism in response to ammonia levels

* Fe protein binds two molecules of Mg ATP

During turnover, ATP hydrolyzed / $2e^-$ ratio is 4 or larger suggesting that thermodynamic efficiency of process ~ 25%

There is a conformational change upon binding of MgATP. Addition of MgATP to Fe-protein shattered the crystals. addition of MgADP did not.

That MgATP binding provokes a <u>conformational change</u> is indicated by EPR of Fe_4S_4 cluster (<u>vide infra</u>)

* <u>Fe_4S_4 cluster</u>

<u>1 Fe_4S_4 cluster per Fe protein</u>

$[Fe_4S_4]^{1+} \xrightarrow{-1e^-} [Fe_4S_4]^{2+} \xrightarrow{-1e^-} [Fe_4S_4]^{3+}$

paramagnetic $S_T = 1/2$	diamagnetic, $S_T = 0$	paramagnetic $S_T = \frac{1}{2}$
reduced ferrodoxin	(oxidized)	oxidized high potential iron-sulfur
S_{12} $Fe^{2.5}\ Fe^{2.5}$ $(\frac{9}{2})$	$Fe^{2.5}\ Fe^{2.5}$ $(\frac{9}{2})$	$Fe^{2.5}\ Fe^{2.5}$ $(\frac{9}{2})$
S_{34} $Fe^{2+}\ Fe^{2+}$ (4)	$Fe^{2.5}\ Fe^{2.5}$ $(\frac{9}{2})$	$Fe^{3+}\ Fe^{3+}$ (5)
S_T $\frac{1}{2}$ also $\frac{3}{2}$	0	$\frac{1}{2}$

antiferromagnetic coupling weak

<u>EPR</u> : $g_{av} = 1.94$

$g_{av} \sim 4.0$

$[Fe_4S_4]^{2+} + e^- \longrightarrow [Fe_4S_4]^{1+}$

<u>Redox potential</u> : -200 mV to -393 mV (versus NHE)

<u>Effect of ATP. Mg (2 equivalents)</u>

Redox potential shifts ~ -120 mV
EPR becomes more axial
} Conformational Change !!

* Crystal structure

Georgiadis, M.M., ... D.C. Rees, Scie 257, 1653-1659 (1992)

→ MoFe protein

* $\alpha_2\beta_2$ tetramer

Molecular mass: ~240 kDa (subunits ca 55 kDa and 60 kDa)

Azotobacter vinelandii: $\begin{cases} \alpha & 491 \text{ amino acids} \\ \beta & 522 \text{ amino acids} \end{cases}$

* Two types of metal center

= 2 FeMo-cofactors (each 1 Mo; 7Fe; $7S^{2-}$)

each FeMo-cofactor consists of one Fe_4S_3 cluster and one $MoFe_3S_3$ cluster bridged by three non-protein ligands also 1 homocitrate coordinated to Mo. ($2S^{2-}$ and 1 O or N);

= 2 P-cluster pairs (each 8Fe; $8S^{2-}$)

each P-cluster pair consists of two Fe_4S_4 clusters bridged by two cysteine residues

for a total of 2Mo; 30 Fe atoms; and $30S^{2-}$.

* Genetics

Gene	Peptide	Function
Q		Mo-processing
B	60K	Synthesis of FeMo-cofactor
V	38-24K	Processing of FeMoco
E	40-46K	Synthesis of FeMoco
Y	19-24K	MoFe protein maturation
K	60K	α-subunit of MoFe protein
D	56K	β-subunit of MoFe protein

* Function of the Clusters

P-clusters are thought to be involved in electron transfer and storage presumably providing a reservoir of low potential electrons to be used by the Fe Mo-cofactor in substrate reduction

Fe Mo-cofactor is the substrate binding and reduction site.

* Crystal structure

J.-S. Kim and D. C. Rees Nature 360, 553-560 (1992)
J.-S. Kim and D. C. Rees Science 257, 1677-1682 (1992)
M. K. Cha, J.-S. Kim and D. C. Rees, Science 258 (1993)

(1) P-cluster

2.2 Å resolution →

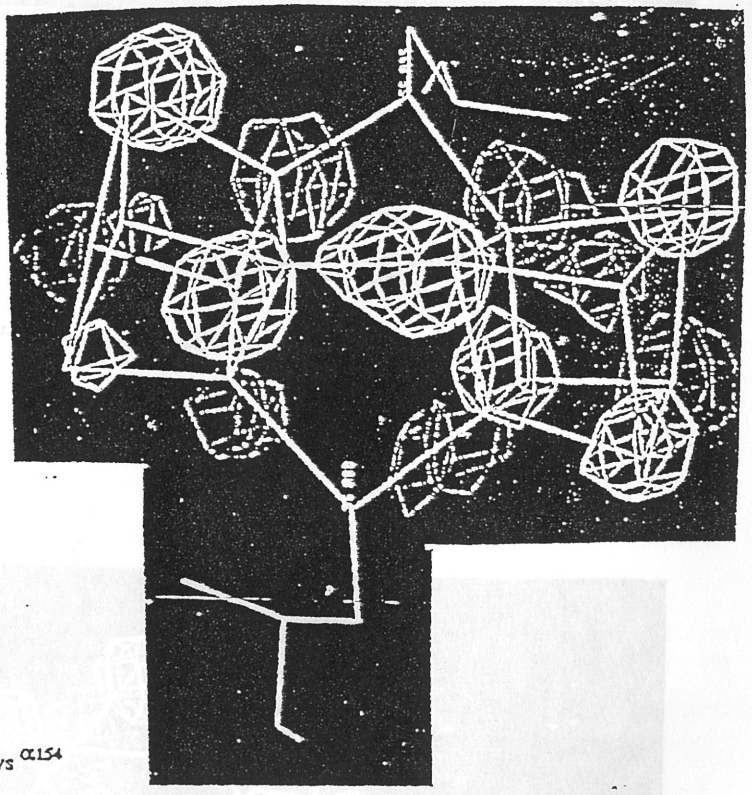

evidence for
$(\mu_3\text{-}S)_2$ disulfide
2.1 Å
(coordinated to 3 Fe's)

2.7 Å resolution ↓

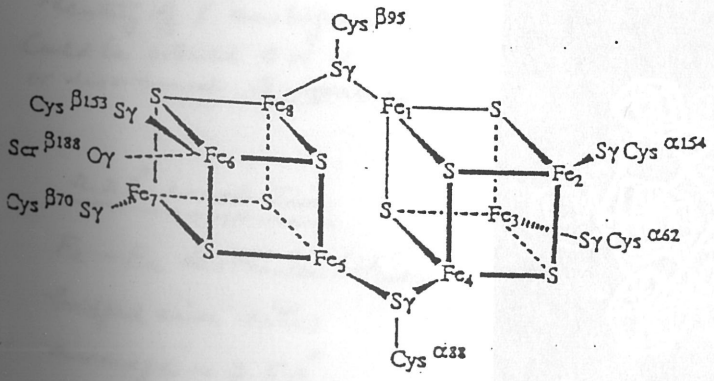

two Fe_4S_4 cubanes linked by two cysteine thiolates (and) from 2.2 Å map → disulfide bond between sulfur atoms in each cluster, i.e., there has been a 2e⁻ oxidation

Upon incubation with CN^-, one of the sulfur atoms is removed by the redox reaction

$$^-S\text{–}S^- + CN^- \longrightarrow S^{2-} + SCN^-$$

thiocyanate

and the electron density in this region is missing!

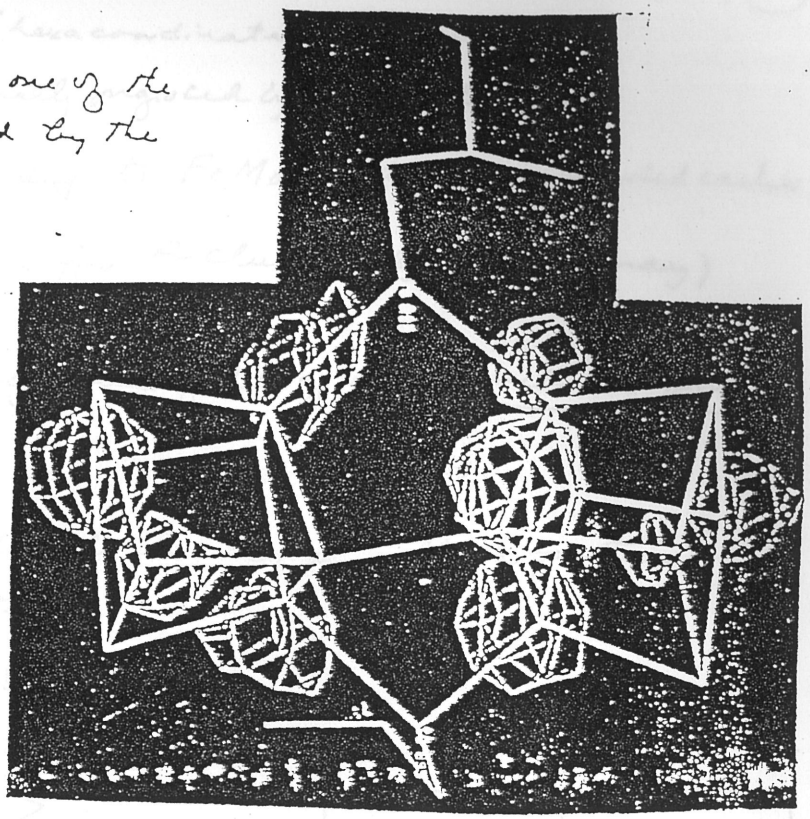

(2) FeMo-cofactor ("M" center)

2.7Å resolution

two MFe_3S_3 ($M \equiv Mo$ or Fe) clusters linked by two bridging sulfides and a third ligand, designated "Y." The chemical identity of "Y" ambiguous! Could be observed O or N or disordered S species.

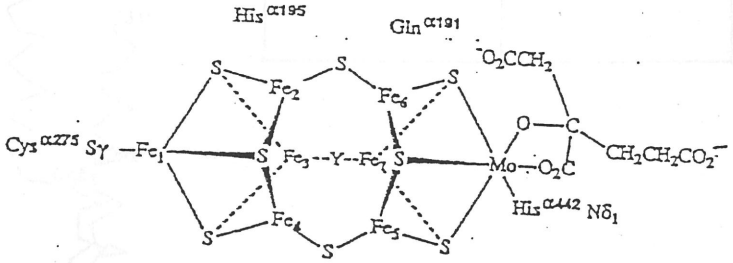

2.2Å resolution

Fe···Fe distances between bridged iron sites average ~ 2.5Å, suggesting that there may be Fe–Fe bonding, with a fourth coordinate ligand ...

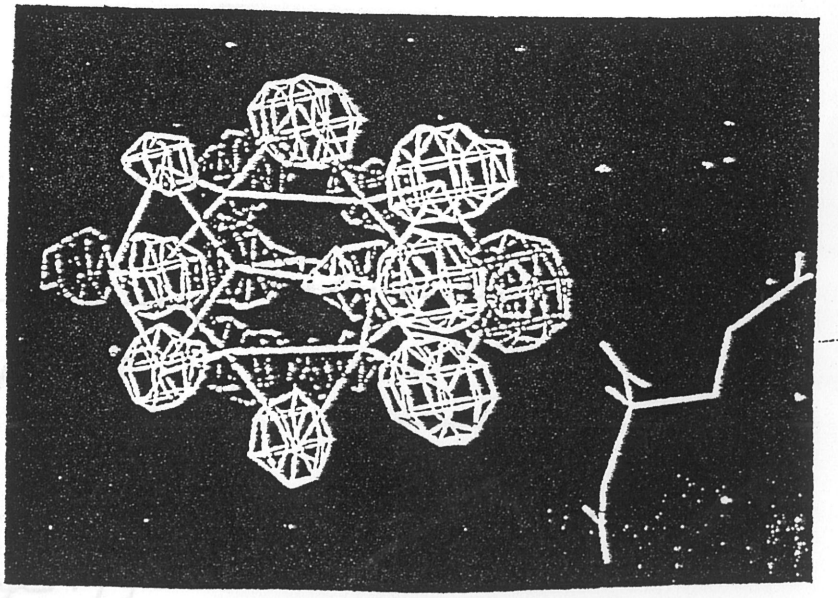

homo-citrate

No evidence of sulfur (hexacoordinated) in center of FeMo-cofactor as originally proposed by Jeff Roli

No evidence of CN^- biding to FeMo-cofactor as proposed earlier.

CN^- biding was observed for P-cluster only (preliminary)

(3) Stereoview of the polypeptide fold of an $\alpha\beta$ subunit pair (page 15)

(4) The polypeptide fold of the $\alpha_2\beta_2$ MoFe protein tetramer pair (partial)

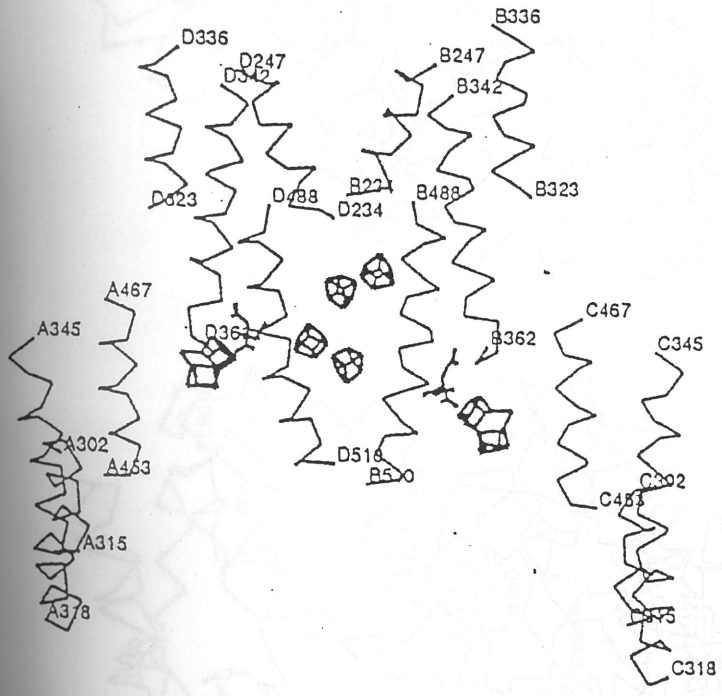

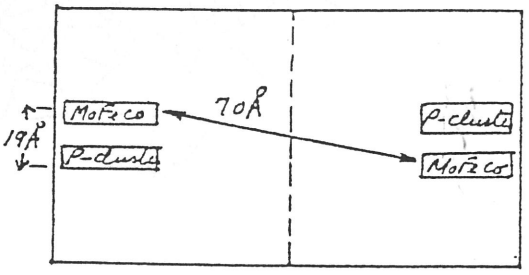

(5) Protein environment surrounding the FeMo-cofactor (see page 16) A

(6) Protein environment surrounding the P-cluster (see page 16) B

(7) Protein environment between FeMo-cofactor and P-cluster (see page 17)

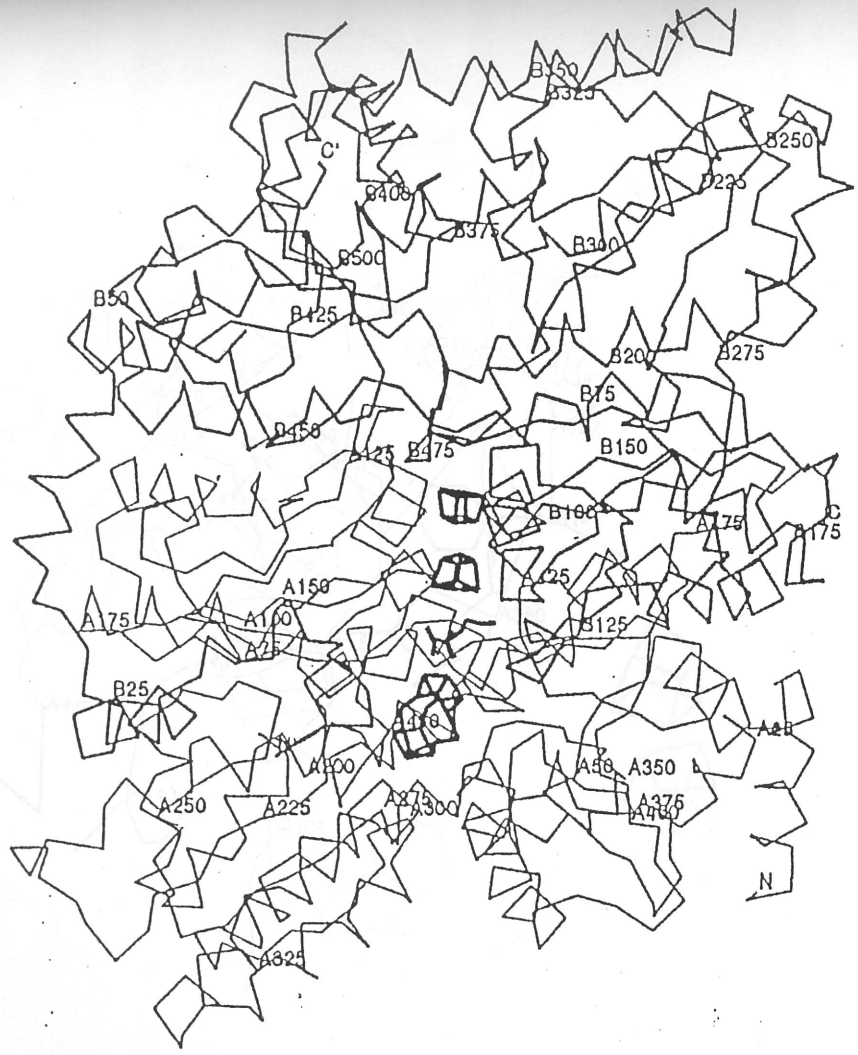
C'
B400
B375
B300
B500
B50
B425
B200
B275
B75
B150
B100
B175
C
A150
A175
A100
A425
B125
B25
A200
A250
A225
A275
A300
A350
A375
A400
N
A325

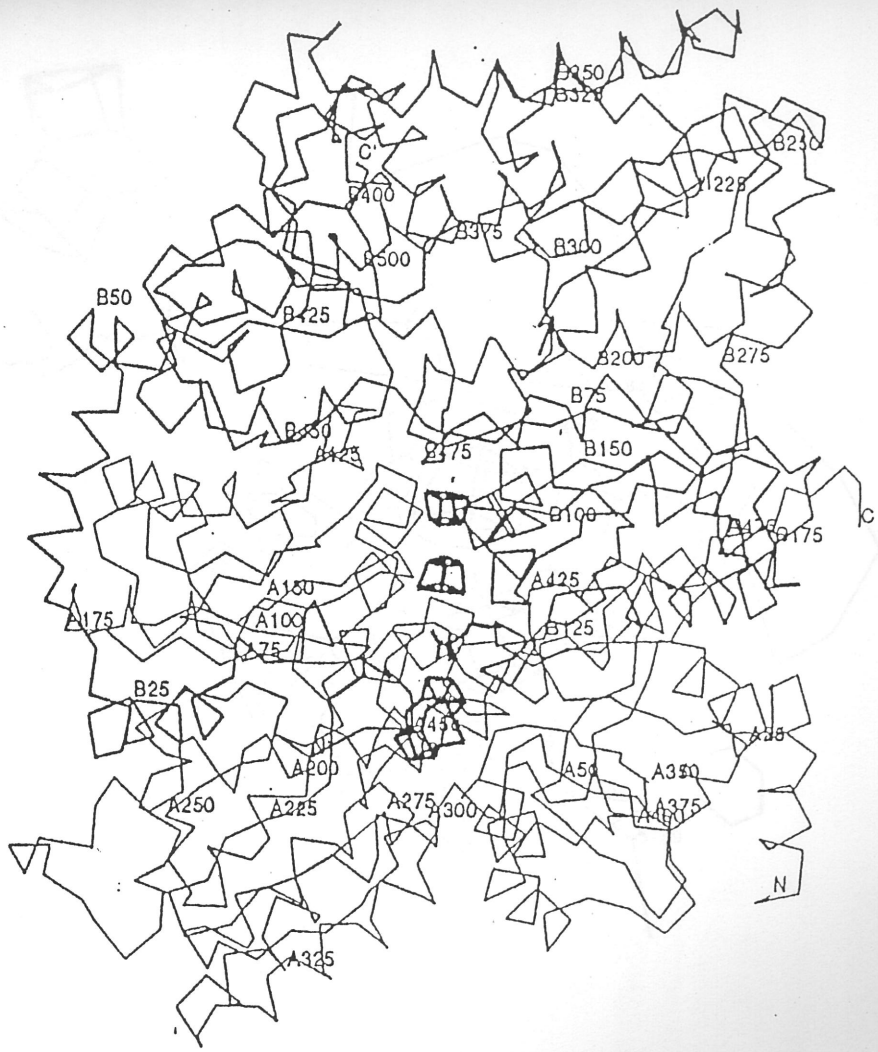
C'
B400
B375
B300
B500
B50
B425
B200
B275
B75
B150
B100
B175
C
A150
A175
A100
A425
B125
B25
A200
A250
A225
A275
A300
A350
A375
A400
N
A325

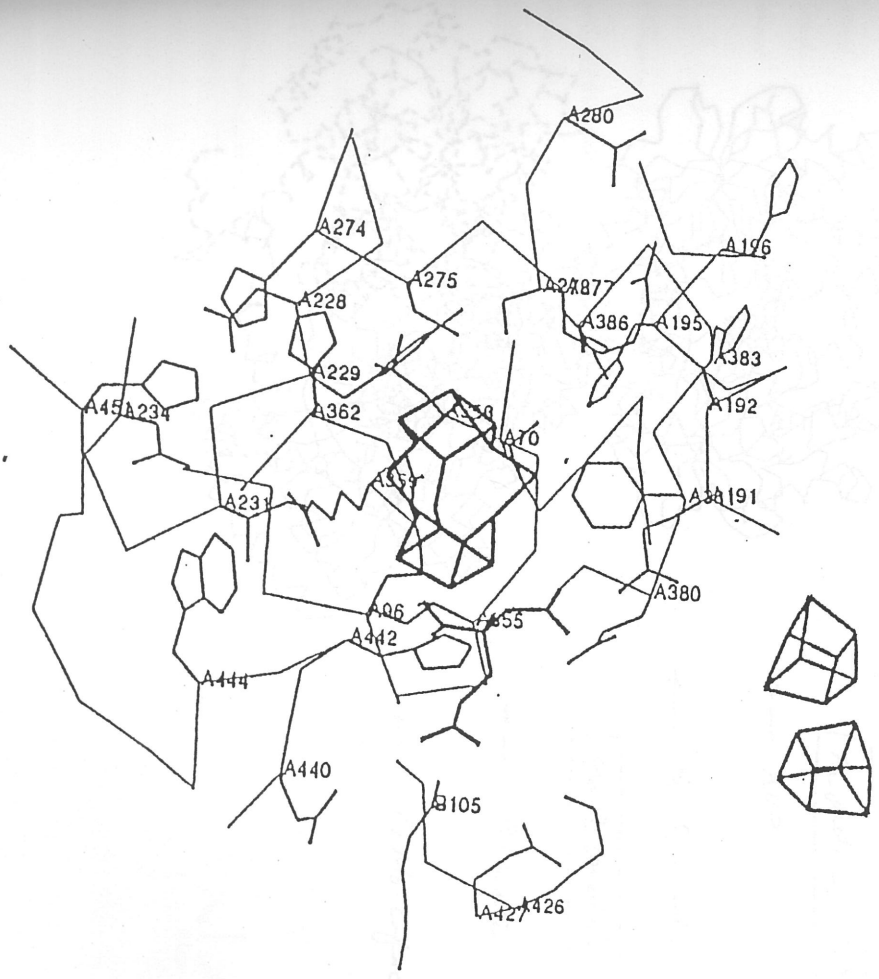
A280
A274
A196
A275
A228
A386
A195
A383
A229
A362
A192
A234
A231
A191
A380
A442
A444
A440
B105
A427
A426

A


A191
A62
A186
A61
B93
A184
B92
A152
A154
A153
B154
A155
B152
B153
A85
B72
B188
B70
B189

B

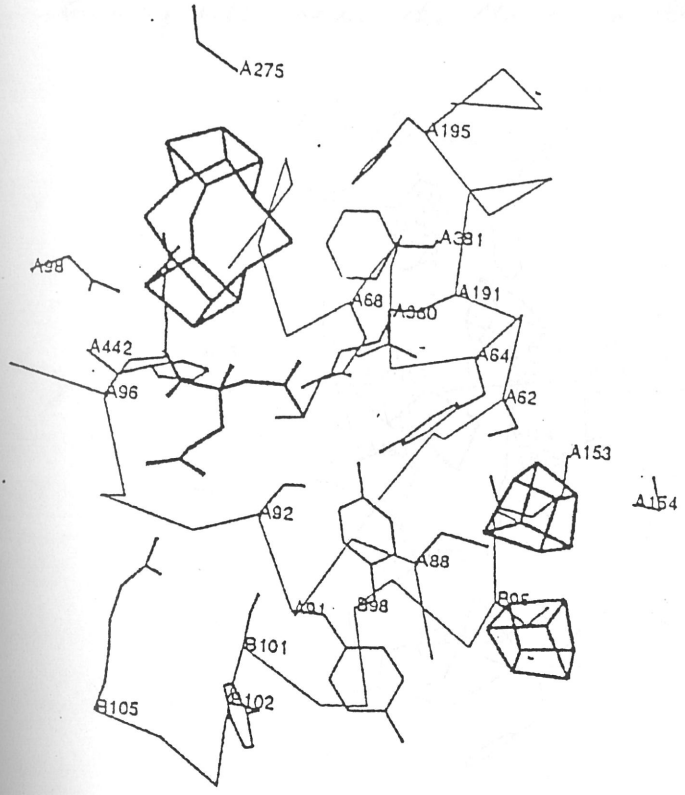

View of
Protein environment
between Fe Mo-cofactor
and P-cluster

* Docking of Fe protein to MoFe protein

(1) C_α model of a complex formed between Fe protein and an $\alpha\beta$ subunit pair of MoFe protein

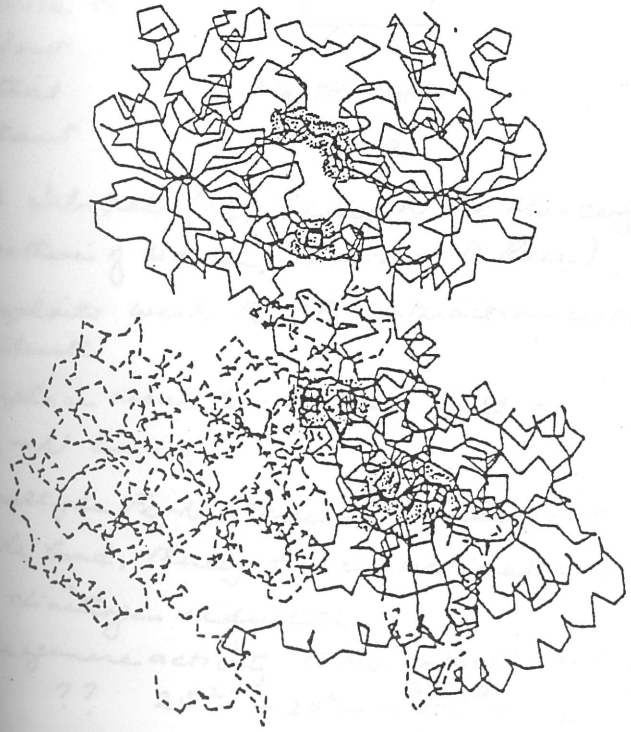

Fe protein (α_2)

← ADP

← Fe_4S_4 cluster

MoFe protein $\alpha\beta$ subunit pair

← P-cluster

← Fe Mo-cofactor

(2) View of the protein environment in the putative Fe-protein binding site, near the Mo-Fe protein P-cluster pair

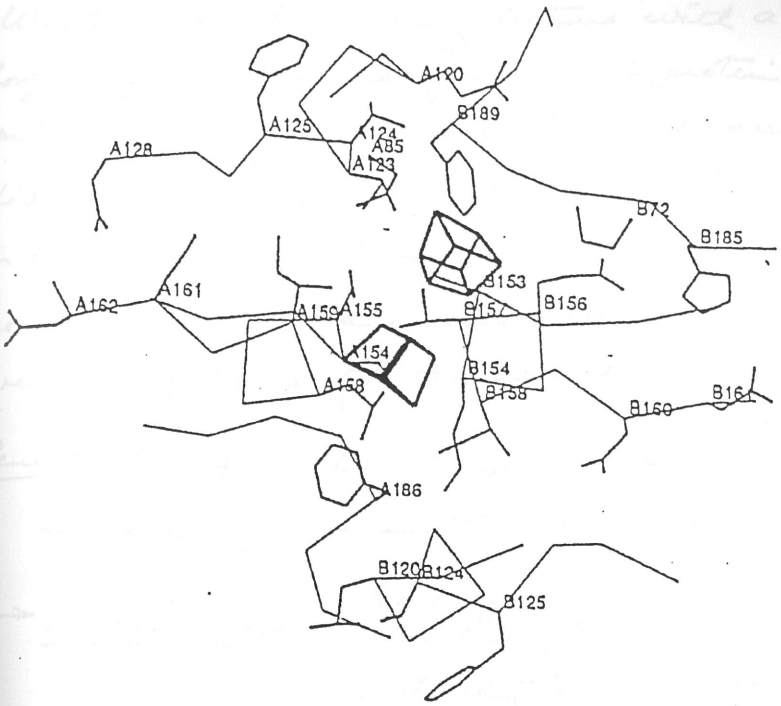

Mo Fe protein

"Interface"

Fe-protein

* Electron transfer and substrate interactions in nitrogenase

(1) Electron flow

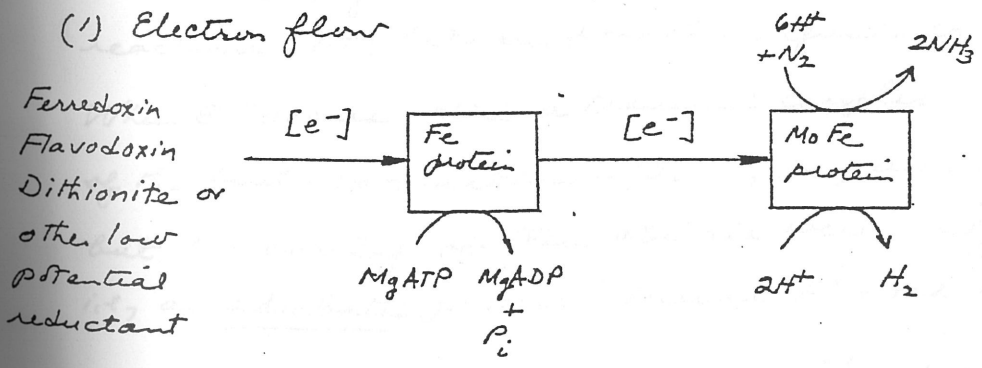

(2) Substrate (N_2) binding to Fe Mo-cofactor

(Hypothesis of M.K Chan, J.-A. Kim & D. Rees)

(a) exploits weak Fe ... Fe interactions within cluster

(b) replace weak Fe ... Fe bonds with multiple Fe–N bonds.

(c) multiple Fe-N interactions weaken $N \equiv N$ triple bond, thereby lowers activation barrier for dinitrogen reduction.

(3) Hydrogenase activity Fe Mo-cofactor or P-cluster

?? $2S^{2-} + 2H^+ \longrightarrow {}^{\ominus}S\text{–}S^{\ominus} + H_2$

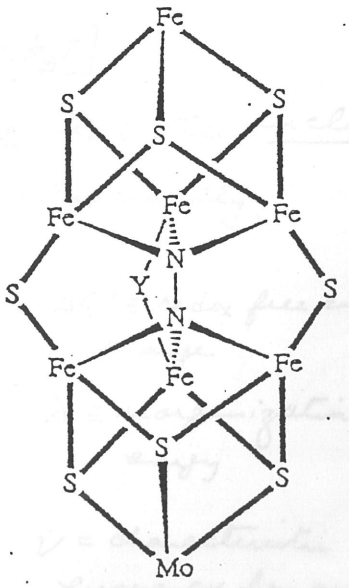

Long-range electron transfer in Protein Systems

We conclude this series of lectures with a brief discussion of long-range electron transfer (ET) in protein systems. Whether a protein is an electron carrier, dioxygen carrier, monooxygenase, dioxygenase, oxidase, nitrogenase or hydrogenase, ET plays a role in the function of the system. Thus, the issue of ET unites all the protein systems discussed in these lectures and is an overarching theme for the course.

General reference "Long-range Electron Transfer in Biology": Structure and Bonding, Volume 75, Springer Verlag, Berlin Heidelberg (1991).

→ Marcus Theory [R.A. Marcus J. Chem. Phys. (1956) 24, 966; J. Chem. Phys. 43, 679 (1960); Dis. Faraday Soc. (1960) 29, 21; R.A. Marcus and N. Sutin, BBA 811, 265 (1985)]

Marcus' original work was concerned with bimolecular reactions (ET) between small inorganic complexes in solution. When ET occurs within a transient complex without disruption of the first coordination sphere, i.e., an outer-sphere process, but the overlap of their orbitals were sufficiently strong, i.e., an adiabatic process, Marcus showed that

$$k_{ET} = \nu \exp-\left[(\Delta G^\circ + \lambda)^2 / 4\lambda k_B T \right]$$

when the temperature is sufficiently high that the nuclear motions of the system can be described classically.

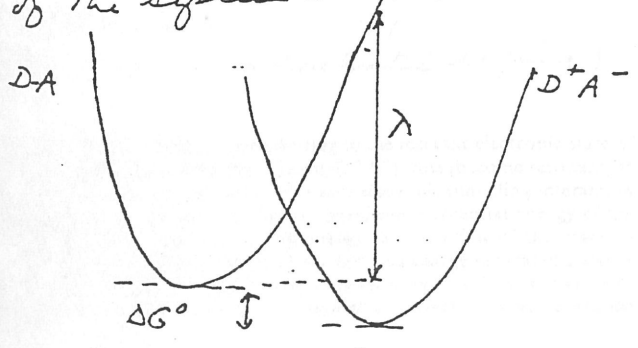

potential surfaces of reactants and products

$\Delta G^\circ \equiv$ redox free energy change

$\lambda \equiv$ reorganization energy

ν = characteristic frequency for nuclear motion

$$\Delta G^\ddagger = \frac{(\Delta G^\circ + \lambda)^2}{4\lambda}$$

The inverted region

→ Marcus' theory predicts that if k_{ET} is studied as a function of the driving force ($-\Delta G^\circ$) for a given D–A pair, the k_{ET} peaks at a driving force $-\Delta G^\circ = \lambda$. For $-\Delta G^\circ < \lambda$, k_{ET} increases with driving force; for $-\Delta G^\circ > \lambda$ k_{ET} decreases with driving force.

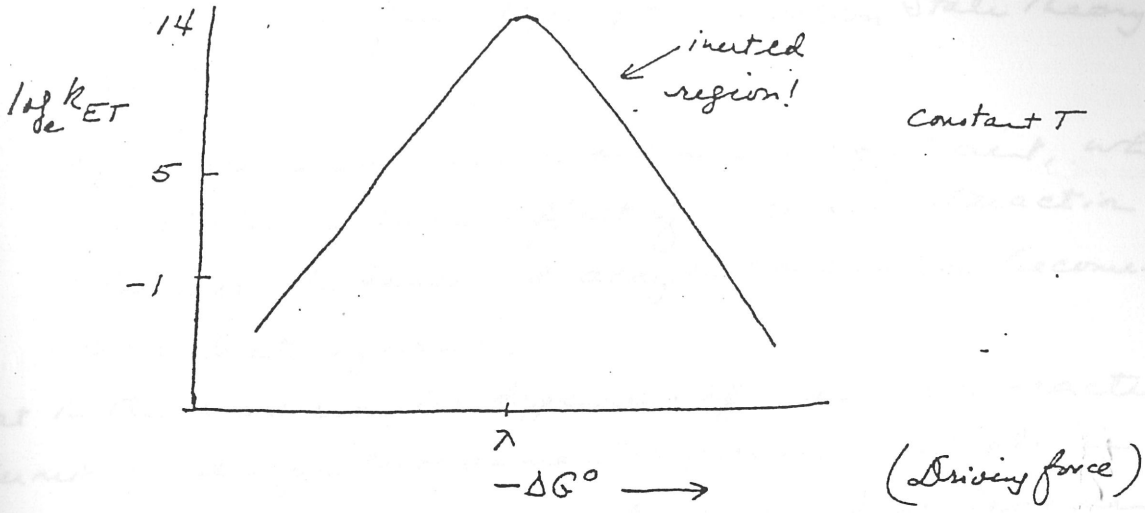

Marcus' prediction of the inverted region was subsequently confirmed by the elegant experiments of G.L. Closs and J.J. Miller [Science 240, 440 (1988); J. Phys. Chem. 90, 3673 (1986); J. Phys. Chem. 93, 1173 (1989)]. It was in recognition of this prediction that Rudy Marcus was awarded the 1992 Nobel Prize in chemistry.

→ A closer look at Marcus' theory

semi-classical
(adiabatic to non-adiabatic regime)

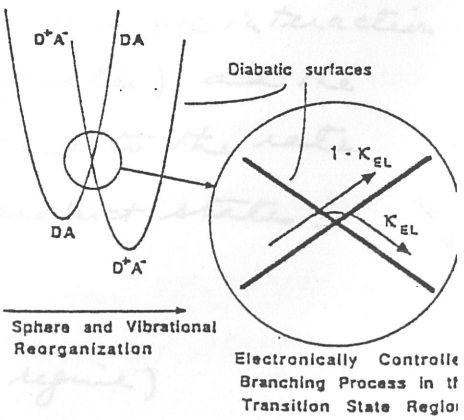

The Marcus parabolic free energy surfaces corresponding to the reactant electronic state of e system (DA) and to the product electronic state of the system (D^+A^-) cross (become resonant) at e transition state. The curves which cross are computed with zero electronic tunneling interaction d are known as the diabatic curves, and include the Born-Oppenheimer potential energy of the olecular system plus the environmental polarization free energy as a function of the reaction ordinate. Due to the finite electronic coupling between the reactant and charge separated states, a iction κ_{el} of the molecular systems passing through the transition state region will cross over onto e product surface; this electronically controlled fraction κ_{el} thus enters directly as a factor into the ctron transfer rate constant

Start with classical transition state theory for the electron transfer rate constant:

$$k_{ET} = \kappa_{EL} A \exp(-\Delta G^{\ddagger}/k_B T)$$

where $\Delta G^{\ddagger}$ is Marcus' classical free energy of activation

A is the adiabatic pre-exponential factor, which may be taken from Eyring's Transition State Theory as $k_B T/h$

κ_{EL} = dimensionless transmission coefficient, which includes the entire effect of electronic interaction between the donor and acceptor (and which becomes crucial at long range).

Note that in this expression, the dependence of rate upon reaction exothermicity and upon environmental polarity controls is reflected in the activation energy and temperature dependence, whereas the dependence on distance, orientation, and electronic interactions between the donor and acceptor is reflected in κ_{EL}.

$0 < \kappa_{EL} < 1$

$\kappa_{EL} = 1$ adiabatic limit

strong quantum mechanical coupling of reactant and product electronic states.

at close range or direct contact, the electronic interaction (Δ) is strong (a few hundred cm^{-1} or greater), and the particular value of Δ is no longer important to the rate

100% cross-over from reactant to product states!

Branching ratio $\kappa_{EL}/(1-\kappa_{EL}) \rightarrow \infty$

κ_{EL} small (as obtains in the non-adiabatic regime)

quantum mechanical coupling of reactant and product electronic states is weak

systems successfully reaching the transition state actually cross into the product state.

The essential physics of this crossover from the adiabatic to non-adiabatic regime is contained in the cross-over formula known as the Landau-Zener transition probability (K_{LZ}) expression.

$$K_{EL} = K_{LZ} = 1 - \exp\left\{ \frac{-\Delta^2 \pi^{3/2}}{\hbar\omega (\lambda k_B T)^{1/2}} \right\}$$

where $\Delta \equiv$ electronic interaction

$\omega =$ frequency of the harmonic potential surfaces

$\lambda =$ reorganization energy.

For very weak coupling limit (Δ small)

$$K_{EL} \cong \frac{\Delta^2 \pi^{3/2}}{\hbar\omega (\lambda k_B T)^{1/2}}$$

and $$k_{ET} = \frac{k_B T}{h} \left(\frac{\Delta^2 \pi^{3/2}}{\hbar\omega (\lambda k_B T)^{1/2}} \right) \exp(-\Delta G^{\ddagger}/k_B T)$$

which is the form predicted from quantum theory for

outer-sphere electron transfer

only very <u>low frequency</u> vibration is excited in

the outer-sphere reorganization

and the high temperature limit is taken

→ <u>Quantum mechanical treatment of problem</u>

Non-adiabatic ET processes

Refs V.G. Levich (1966) Adv. Electrochem. Electrochem Eng. 4, 249

R.R. Dogonadze, A.M. Kuznetsov, M.A. Vorotyntsev (1972) Phys. Stat. Sol. B. 54, 125

N.R. Kestner, J. Logan, J. Jortner (1974) J. Phys. Chem 78, 2148

J.J. Hopfield (1974) Proc. Natl. Acad. Sci. USA 71, 3640

J. Jortner (1976) J. Chem. Phys. 64, 4860

Assume that the potential surface of the initial D-A state can be written as

$$H_{aa} = C + \sum_n \tfrac{1}{2} k_n (Q_n - Q_{na})^2$$

and the potential surface of the product $D^+ - A^-$ state can be written as

$$H_{bb} = C + \sum_n \tfrac{1}{2} k_n (Q_n - Q_{nb})^2 + \Delta U^\circ$$

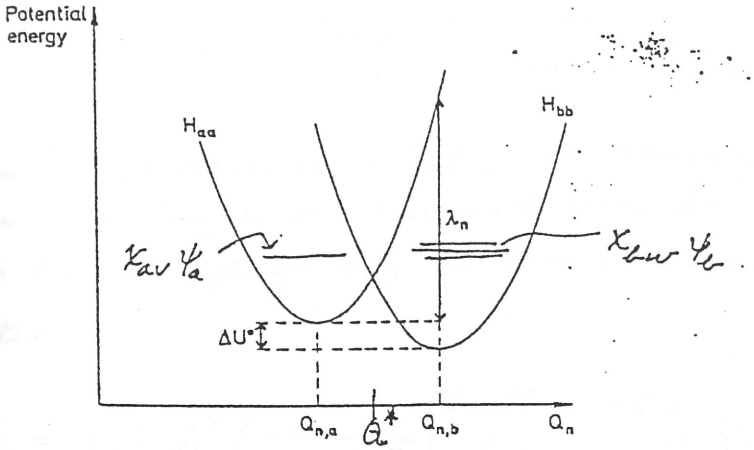

Definition of the contribution λ_n to the reorganization energy. The figure represents the variations of the potential energy when only Q_n is varied, the other coordinates being kept constant at their equilibrium values

Then the reorganization energy, i.e., the energy that has to be supplied to the system to change the oscillator coordinate from $Q_{n,a}$ to $Q_{n,b}$ when it is in state ψ_a (reactant D-A state), is $\lambda_n = \tfrac{1}{2} k_n (Q_{nb} - Q_{na})^2$

The problem is to calculate the transition probability per unit time from the initial state $\chi_{av}\psi_a$ to the isoenergetic continuum of states $\chi_{bw}\psi_b$

vibration electronic — vibration electr

According to Fermi "Golden rule",

$$W(av \to bw) = \left(\frac{2\pi}{\hbar}\right) \left| \int_Q \chi^*_{bw}(Q)\, V_{ba}(Q)\, \chi_{av}(Q)\, dQ \right|^2 \rho(E_{bw})$$

where $V_{ba} = \int \psi_b^* V(Q) \psi_a \, d\tau_e \equiv \Delta$

and $\rho(E_{bw})$ = density of final states

This treatment applicable when V_{ba} is sufficiently weak for

perturbation treatment to be valid. Otherwise, rate becomes independent of these interaction, if the interaction is strong enough for the reaction to move into adiabatic region

Now if $V_{ab}(Q)$ vary slowly with Q in the transition region $Q \sim Q^*$ where χ_{aV} and χ_{bW} overlap significantly, then

$$W(aV, bW) = \underbrace{\left(\frac{2\pi}{\hbar}\right)|V_{ba}|^2}_{\Delta^2} \underbrace{\int_Q \chi^*_{bW}(Q)\,\chi_{aV}(Q)\,dQ\Big|^2}_{\text{Franck Condon factor}} \rho(E_{bW})$$

(a) When ET process is coupled to classical reorientation modes and to only one harmonic oscillator whose energy quanta $\hbar\omega_v$ is high enough for only the ground vibrational level to be populated,

$$k_{ET} = \left(\frac{2\pi}{\hbar}\right)\Delta^2\left(\frac{1}{4\pi\lambda_S k_B T}\right)^{1/2}\sum_{m=0}^{\infty} e^{-S}\left(S^m/m!\right)\exp\left[-\frac{(\lambda_S + m\hbar\omega_v + \Delta G^\circ)^2}{4\lambda_S k_B T}\right]$$

where $S = \dfrac{\lambda_v}{\hbar\omega_v}$,

λ_S = contribution to reorganization energy arising from dielectric medium

λ_v = contribution to reorganization energy from oscillator

(b) When the temperature is sufficiently high so that all nuclear motions can be treated classically, then

$$k_{ET} = \left(\frac{2\pi}{\hbar}\right)\Delta^2\left(\frac{1}{4\pi\lambda k_B T}\right)^{1/2}\exp\left(-\Delta G^*/k_B T\right)$$

where $\Delta G^* = \dfrac{(\Delta G^\circ + \lambda)^2}{4\lambda}$

and λ = the total reorganization energy
$= \lambda_i + \lambda_o$

λ_i = due to redox center

λ_o = due to medium, protein

(c) V_{ba} or Δ

Experimentally, it is found that

$$|V_{ba}|^2 = \Delta^2 \propto (\exp -\alpha R)^2 = \exp -2\alpha R$$

where R = donor-acceptor distance

and $\alpha \simeq 0.5$ to $0.7\ \text{Å}^{-1}$ when D & A are embedded or dispersed in a rigid matrix glass or polymer.

$\alpha \simeq 0.4$ to $0.5\ \text{Å}^{-1}$ when D and A are connected by rigid covalent linker of bonds

This value of α is consistent with superexchange model of electronic coupling via bonds in the linker or solvent medium.

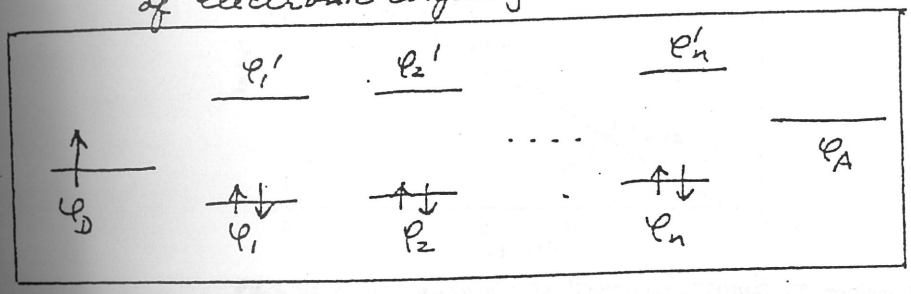

→ Experimental Method for Studying Long-Range ET in Protein.

(1) The method of Harry Gray (exploiting Ru-modified proteins)

(a) ET from a surface as Ru (III)(histidine) to a protein redox center

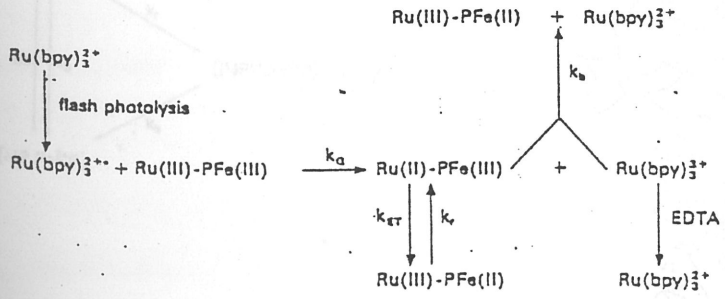

Scheme: Flash photolysis method for studying $Ru^{II} \rightarrow Fe^{III}$ ET.

Table 1. ET [Ru(II) → Fe or Cu acceptor] in a_3Ru(HisX)-Modified Proteins

Protein	X	Acceptor	d(Å)	$-\Delta G^*$(eV)	$k_{ET}(s^{-1})$
Cytochrome *c* (horse heart)[a]	33	Fe(III)	11.7	0.18	30 ± 3 (53 ± 2)[b]
Cytochrome *c* (*Saccharomyces cerevisiae*)[c]	62	Fe(III)	15.6	0.20	1.7 ± 1
Cytochrome c_{551} (*Pseudomonas stutzeri*)[d]	47	Fe(III)	7.9	0.20	13 ± 2
Myoglobin (sperm whale)[e]	48	Fe(III)	12.7	− 0.02	0.019 ± 0.002
Azurin (*Pseudomonas aeruginosa*)[f]	83	Cu(II)	11.8	0.24	1.9 ± 0.4 (2.5 ± 0.8)[g]
Plastocyanin (*Anabaena variabilis*)[g]	59	Cu(II)	11.9	0.26	< 0.08
Plastocyanin (*Scenedesmus obliquus*)[g]	59	Cu(II)	10–12	0.29	< 0.26
Stellacyanin (*Rhus vernicifera*)[h]	32/100	Cu(II)	—	0.104	0.05
HIPIP (*Chromatium vinosum*)[i]	42	Fe_4S_4	7.9	0.27	18 ± 2

(b) ET from an electronically excited metalloporphyrin ($^3MP^*$) to a a_5Ru(III) (histidine) on protein surface

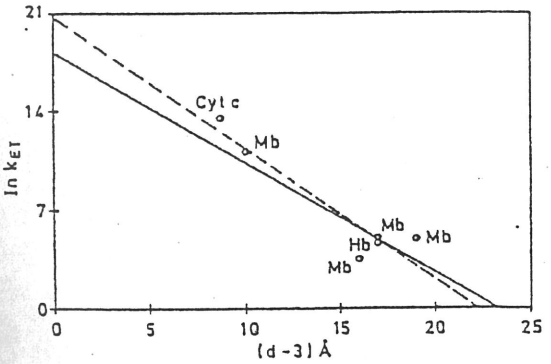

$\beta = 2\alpha$

Fig. 2. Ln k_{ET} *vs.* distance plot for $^3ZnP^* \rightarrow a_3Ru(III)(HisX)$ ET reactions in ruthenated sperm whale myoglobin [31, 33]: Mb, X = 48, 81, 116, 12; also shown are points for cyt *c* [$^3ZnP^* \rightarrow a_3Ru(III)(His33)$] [34] and Zn,Fe–Hb [$^3ZnP^* \rightarrow Fe(III)P$] [35]. *Solid line*, $\beta = 0.78$ Å^{-1}; *dashed line*, $\beta = 0.93$ Å^{-1}

(2) The Method of Bria Hoffman (exploiting Metal-substituted Protein Complexes)

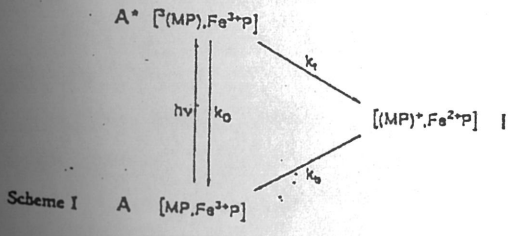

Scheme I

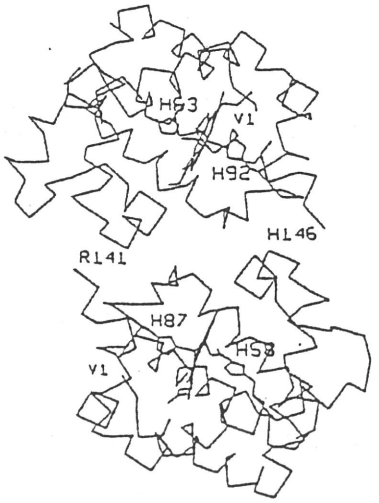

α-Carbon backbone of an $[\alpha_1\beta_1]$ dimer within the $[\alpha(FeCO)P, \beta(Mn^{3+}P)]_2$ hybrid. (From Ref. [13])